Gearbox Reliability Collaborative
Analytic Formulation for the Evaluation of Spline Couplings

Yi Guo and Jonathan Keller
National Wind Technology Center
National Renewable Energy Laboratory

Robert Errichello
GEARTECH

Chris Halse
Romax Technology

Acknowledgments

This work was supported by the U.S. Department of Energy under contract number DE-AC36-08GO28308 with the National Renewable Energy Laboratory. The authors would also like to thank Jan Helsen of the Katholieke Universiteit Leuven for her advice in developing the research topic, Jason Austin and Donald Houser from The Ohio State University for providing the Transmission 3D model of the spline, Sandeep Vijayakar from Advanced Numerical Solutions for developing the conformal contact functionality in Transmission 3D, and Sharad Jain from Romax Technology for valuable discussions regarding spline contact properties.

List of Acronyms

2D	two-dimensional
3D	three-dimensional
AGMA	American Gear Manufacturers Association
FE	finite element
GRC	Gearbox Reliability Collaborative
GUI	graphical user interface
IEC	International Electrotechnical Commission
NREL	National Renewable Energy Laboratory
SCouP	Spline Coupling Program

Nomenclature

C	Bending stiffness of a single pair of spline teeth
C_ψ	Helical overlap ratio
D_o	Hub major diameter
D_i	Sleeve minor diameter
E	Young's modulus
F	Facewidth
f_c	Half tooth facewidth in contact
h	Hub tooth tip chamfer
h_1	Active tooth flank height
h_F	Height of Lewis parabola
$i, i_d, i_{\max}$	Misalignment angle, design misalignment angle, and jam angle
J	Geometry factor
K	Accuracy factor
K_a	Surface factor
K_b	Size factor
K_c	Reliability factor
K_d	Temperature factor
K_e	Stress concentration factor
K_f	Hub tooth AGMA stress correction factor
K_m	Miscellaneous effects factor
k_R	Rotational stiffness of a single pair of spline teeth

K_v	Velocity factor
m_N	Coupling load sharing ratio
n	Safety factor
N	Number of spline teeth
n_{bf}, n_{cf}, n_{sf}	Bending, contact, and shear fatigue safety factors
n_{by}, n_{cy}, n_{sy}	Bending, contact, and shear yield safety factors
P	Diametral pitch
P_d	Normal tooth load carried by the teeth adjacent to the highest-loaded tooth
P_i	Normal tooth load carried by the highest-loaded tooth
P_i'	Normal tooth load carried by the highest-loaded tooth, per unit length
P_t	Total normal tooth load
q	Number of teeth in contact
R	Pitch radius
R_c	Hub root crown radius at pitch diameter
R_F	Hub face crown radius (normal plane)
S_{bf}, S_{cf}, S_{sf}	Bending, contact, and shear endurance strength
S_{by}, S_{cy}, S_{sy}	Bending, contact. and shear yielding strength
S_{c2}	Design sleeve circular space width
$S_e, S_e^{'}$	Modified and absolute bending endurance strength
S_F	Tooth thickness at the critical section
S_u	Tensile strength
S_y	Yielding endurance strength
T	Transmitted torque

t_{c1}, t_{c2}	Hub and sleeve tooth circular thickness
t_{c1}^{*}	Hub tooth circular thickness at the contact point
W_t	Tangential tooth load
Y_1, Y_2	Hub and sleeve tooth AGMA form factor
Z_1, Z_2	Hub and sleeve elasticity factor
z	Elastic tooth deformation of the teeth adjacent to the highest-loaded tooth
z_o	Maximum tooth separation
z_e	Maximum elastic tooth deformation of the highest-loaded tooth
ϕ	Normal pressure angle
σ_a	Alternating stress
σ_b	Bending stress
σ_c	Contact (Hertzian) stress
σ_e	Effective distortion energy stress
σ_m	Mean stress
τ	Shear stress
ρ_F	Minimum radius of curvature of the fillet curve

Table of Contents

List of Figures

List of Tables

1 Introduction

1.1 GRC Overview

Many gearboxes in wind turbines have not been achieving their expected design life [1]; however, they commonly meet and exceed the design criteria specified in current standards in the gear, bearing, and wind turbine industry as well as third-party certification criteria. The cost of gearbox replacements and rebuilds, as well as the downtime associated with these failures, has elevated the cost of wind energy. The National Renewable Energy Laboratory (NREL) Gearbox Reliability Collaborative (GRC) was established by the U.S. Department of Energy in 2006; its key goal is to understand the root causes of premature gearbox failures and improve their reliability using a combined approach of dynamometer testing, field testing, and modeling [2]. One of the basic premises of the NREL GRC is that the gap between design-estimated and actual wind turbine gearbox reliability is caused by an underestimation of loads, inaccurate design tools, the absence of critical elements in the design process, or insufficient testing. One of the overall goals of the GRC is to facilitate an increase in the accuracy of existing gearbox design and modeling tools, or to produce these tools when none are available. Another goal is to make recommendations to improve gearbox design standards.

1.2 Study Motivation

As part of the GRC program, this paper investigates the design of the spline coupling often used in modern wind turbine gearboxes to connect the planetary and helical gear stages. The GRC gearbox configuration with the sun spline is shown in Figure 1. Aside from transmitting the driving torque, another common function of the spline coupling is to allow the sun to float between the planets. The floating principle equalizes the load distribution between planets as

much as possible, given the realities of imperfections such as machining errors and misalignment and loads imparted to the planetary system other than torque alone. A freely floating sun minimizes the negative effect of these realities on the planet, sun, and ring gear mesh contact patterns. Conversely, without the floating sun, gearbox misalignment and unequally shared loads can occur. As a result, edge loading of the gears and planet-bearing forces increase, leading to reduced gear and bearing life and potential premature failure [3].

The amount the sun can float is determined by the spline design and the sun shaft flexibility subject to the operational loads. American Gear Manufacturers Association (AGMA) 6006-A03 [4], AGMA 6123-B06 [5], and IEC 61400-4 [6] address spline coupling design requirements in varying detail, with the most detailed guidance provided in AGMA 6123-B06 for single articulation couplings. This report provides additional insight beyond these current standards to help quickly evaluate spline coupling designs.

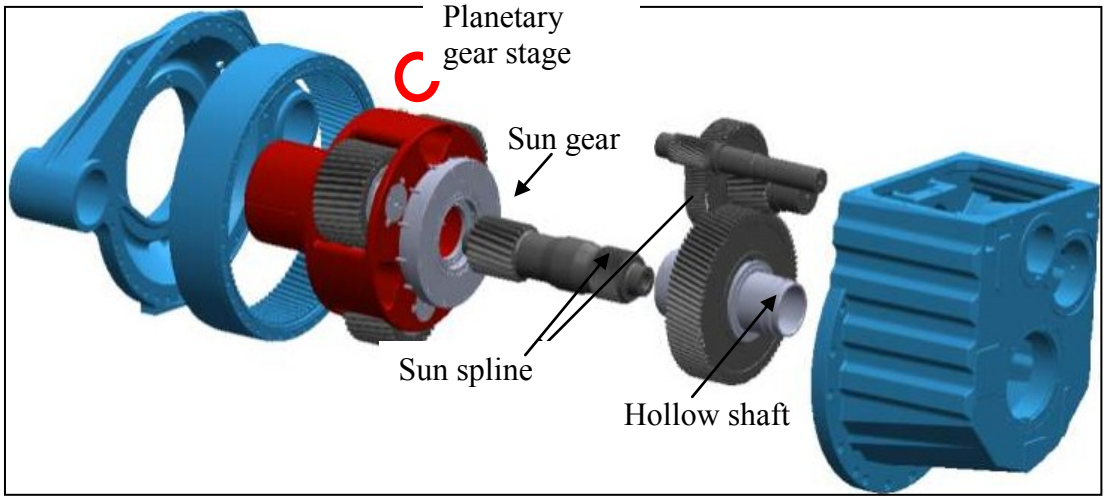

Figure 1. Gearbox configuration. ***Illustration by Powertrain Engineers Inc.***

The following sections provide additional motivation for investigating the design and modeling of the sun spline.

1.1.1 GRC Survey of Designers

One of the overall goals of the GRC is to facilitate an increase in the accuracy of existing gearbox design and modeling tools, or to produce these tools when none are available. To collect objective insights into the important issues that wind turbine gearbox designers are facing, a blind survey was distributed by the GRC in late 2011 to the designers of leading wind turbine gearbox firms. A portion of the survey was dedicated to gathering opinions regarding the gearbox components for which design methodologies are either not mature enough to yield sufficient reliability or have limited availability. The design of the sun spline was commonly mentioned as one of these components. Therefore, the GRC program began to collect expert opinions on the features of a tool that would be most valuable to the industry.

1.1.2 GRC Damage Analysis

One of the GRC gearboxes was installed in a turbine at the Ponnequin wind farm in September 2009 to gather field loading data. After approximately 1 month, the test was stopped because of

bearing temperature exceedances and reports of oil loss from the gearbox. An inspection revealed that the high-speed stage gear teeth showed signs of significant overheating. As a result, testing was suspended to avoid the potential for catastrophic gearbox failure. Subsequently, the gearbox was removed from the turbine and shipped back to NREL. After conducting a limited set of condition monitoring tests in the NREL dynamometer, the gearbox was disassembled and inspected [7].

Some of the noted damage to the gearbox was related to the sun spline connection. The primary damage to the sun spline was the severe fretting corrosion shown in Figure 2 and Figure 3. The root cause of this damage was probably poor load sharing and lubricant starvation. The fretting corrosion was concentrated on about half of the spline teeth, indicating that about half of the teeth were carrying the torque load. It was recommended by the GRC gearbox designer to increase the accuracy of the spline teeth to improve the tooth-to-tooth load distribution.

Figure 2. Fretting corrosion of the sun spline. ***Photo by Robert Errichello, GEARTECH, NREL 19852***

Adhesion between the external sun spline and the hollow shaft internal spline transferred lumps of material from the hollow shaft as shown in Figure 3. Axial sliding broke the welds and deformed the material in the axial direction. The red debris is hematite (Fe_2O_3), a polishing agent that created polishing wear that surrounds the fretting damage.

Figure 3. Close-up of fretting corrosion of the sun spline. ***Photo by Robert Errichello, GEARTECH, NREL 19853***

1.1.3 Other Reliability Analysis and Prediction Results

The estimated failure rates of different gearbox subcomponents for several representative wind turbines were reported in the framework of the Reliawind project and are listed in Table 1 [8]. The sun spline failure rate in this analysis was similar to other planetary system gears and bearings. In addition to the outright failure of the sun spline itself, poorly functioning splines could also be a contributor to failures in the rest of the planetary stage because of their influence on load-sharing characteristics.

Table 1. Estimated Failure Rate of the R80 Turbine Planetary System [8]

Part	Failure Rate (failures/year)	Quantity
Low Speed Shaft	0.00250	1
Low Speed Shaft Bearing	0.00009	2
Planet Shaft	0.00250	3
Planet Bearing	0.00022	3
Planet Gear	0.00017	3
Ring Gear	0.00017	1
Sun Pinion	0.00017	1
Sun Shaft	0.00250	1
Sun Spline	0.00025	1

1.2 Objective

Based on the GRC survey and considerable spline failure rate of the R80 turbine, it appears that the current spline design methods are not sufficient for wind turbine gearbox systems. As a result, there is an opportunity for the GRC program to develop a greater understanding of spline modeling, contribute to design methodologies, and positively influence spline design standards.

The objective of this report is to describe a simple, analytical formulation for quick spline coupling design and spline coupling rating analysis. The formulation has been coded into software and is compared to existing higher fidelity spline coupling modeling tools. This analytic formulation provides essential design information and could be easily integrated into gearbox design and simulation tools. The formulation also provides insight into the effect of spline design parameters on the spline behavior, some of which are not discussed in the current gearbox design standards.

2 GRC Test Article and Instrumentation

The GRC test article drivetrain originally was designed for a two-speed, stall-controlled, three-bladed upwind turbine with a rated power of 750 kilowatts (kW) [1]. The design follows a conventional configuration wherein all the drivetrain components are mounted onto the bed plate. These components include the hub, main bearing, main shaft, gearbox, brake, generator shaft, and generator as shown in Figure 4. Everything but the hub is included in the dynamometer tests. The drivetrain follows a common configuration of megawatt-scale turbines used in the industry today. The gearbox is mounted with a three-point configuration in which torsional loads are transferred to the main frame through two torque arms, and forces are reacted mostly at the main bearing.

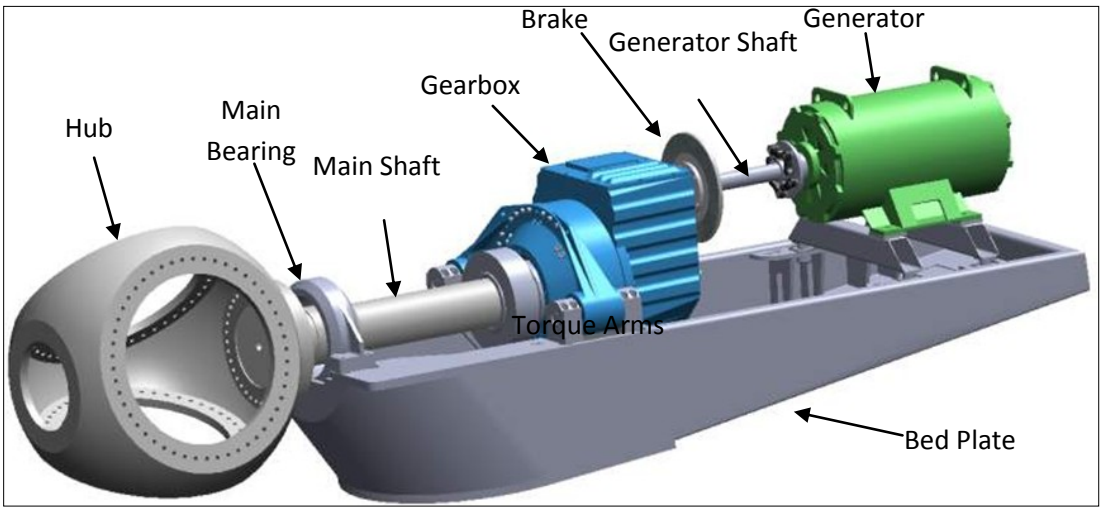

Figure 4. Drivetrain configuration

The gearbox is composed of one low-speed planetary stage, accommodating three planet gears, and two parallel shaft stages as shown in Figure 1. The gears and bearings were redesigned and have been modified from the original gearbox configuration used in the commercial versions of this wind turbine. This redesigned gearbox is hereafter termed the "the GRC gearbox."

In the GRC gearbox, the sun gear is in a floating configuration to equalize the load distribution among the planets. The sun gear is integral to a long shaft with an external spline (hub) on its downwind end as shown in Figure 1. The hub is connected to the hollow low-speed shaft (sleeve) through an internal spline. The spline coupling is a single articulation design with significant crowning. Key parameters of the external spline (hub) are listed in Table 2. The spline carries an operational torque of 57 kiloNewton meters (kNm) (504,000 lb-in) that is transferred to the parallel-shaft stages.

Table 2. Sun Spline Coupling Specified Geometry

Parameter	Symbol	Value
Hub major diameter, inch	D_o	8.42
Sleeve minor diameter, inch	D_i	7.80
Effective facewidth, inch	F	4.61
Number of teeth	N	48
Diametral pitch, 1/inch	P	6
Pitch radius, inch	R	4.00
Hub face crown radius, inch	R_F	444.97
Hub circular tooth thickness, inch	t_{c1}	0.285 – 0.286
Sleeve circular tooth thickness, inch	t_{c2}	0.225 – 0.226
Normal pressure angle, degree	ϕ	20.00
Lead modification type		Lead full crown
Heat treatment technique for hub		Carburized
Heat treatment technique for sleeve		Nitrided

The GRC gearbox is highly instrumented both internally and externally [9]. Of special interest in this work is the measurement of the main shaft torque and bending, plus the radial position of the sun gear relative to the planet carrier. This radial motion is measured using two orthogonal proximity sensors mounted on the planet carrier as shown in Figure 5 and Figure 6. The sensors discern the upwind end of the sun shaft in the area of the shaft that extends about 50 mm beyond the end of the sun pinion. There is no direct measurement acquired on the spline itself because of the challenges of instrumentation and wiring.

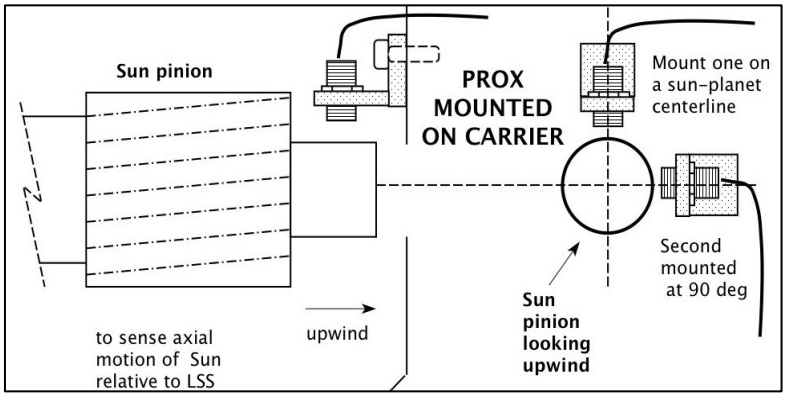

Figure 5. Sun proximity sensor schematic. ***Illustration by McNiff Light Industry***

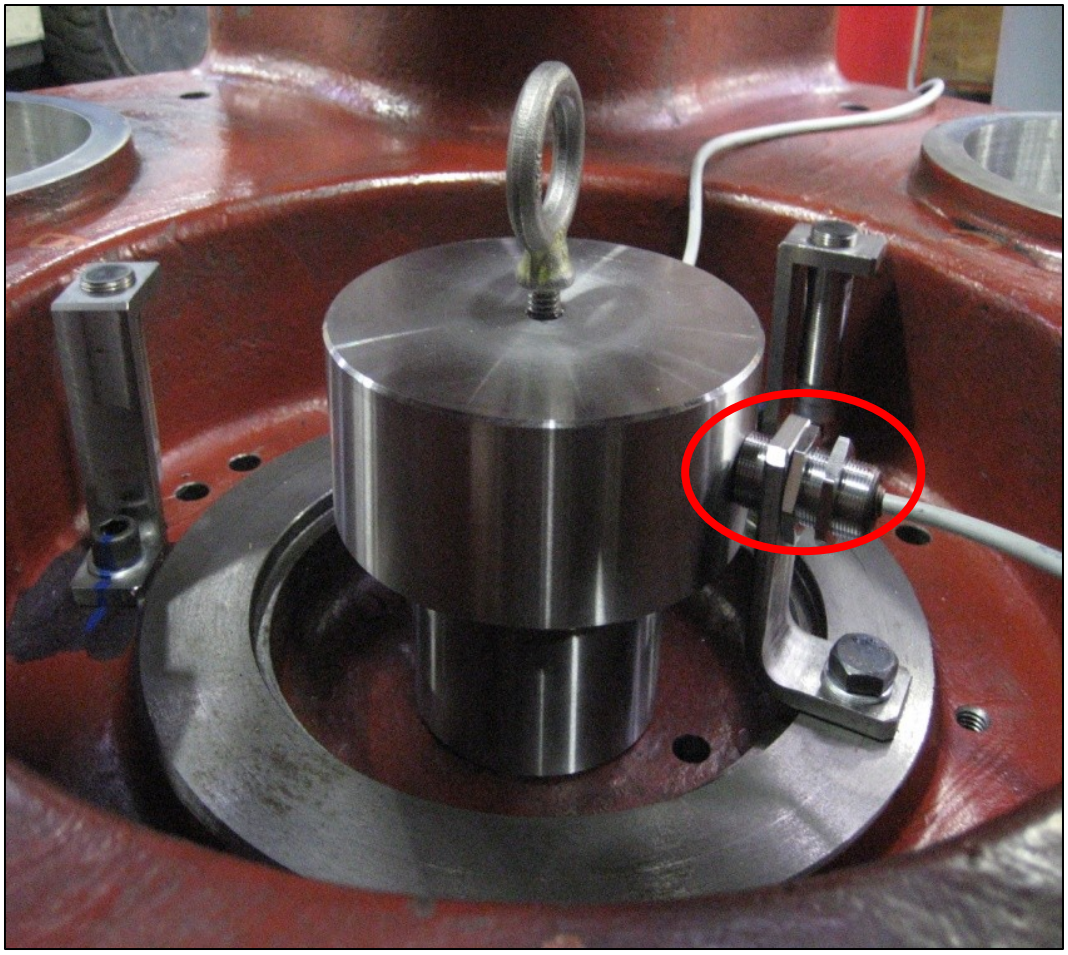

Figure 6. Sun proximity sensor (one of two sensors). ***Photo by Edward Overly, NREL 26666***

The sun gear orbiting motion measured during the dynamometer testing is shown in Figure 7. The measurement was taken at rated torque (325 kNm) and two amplitudes of main shaft pitching moments (also called non-torque loads). Aerodynamics loads and turbine gravity forces cause non-torque loads transmitted into the main shaft. Pitching moments tilt the planetary gears and cause unequal planetary load sharing [10]. In order to accommodate this tilt, the sun spline allows the sun shaft to self-adjust and orbit near freely in the planetary system plane. As a result, the sun orbiting motion increases with pitching moment significantly. The sun gear has up to 0.25 mm of orbiting motion about the spline tooth center. Assuming this motion results only in angular misalignment, the sun shaft misalignment is up to 0.023° as shown in Figure 7. AGMA 6123-B06 recommends a reasonable limit of 0.057° (0.001 radian) for a single articulation coupling, which is slightly over double the measured misalignment.

The pitching moments measured in field tests were much higher (275 kNm) than the maximum applied during the dynamometer tests (125 kNm) [9]. Therefore, it is expected that sun orbiting motion occurring in the field is even higher than measured during the dynamometer test. The frequency spectrum of the sun orbit, shown in Figure 7, consists of higher-energy resonances at the planetary rotation frequencies than the energy at the planet-sun mesh frequency, which suggests potential manufacturing deviations and misalignments might exist.

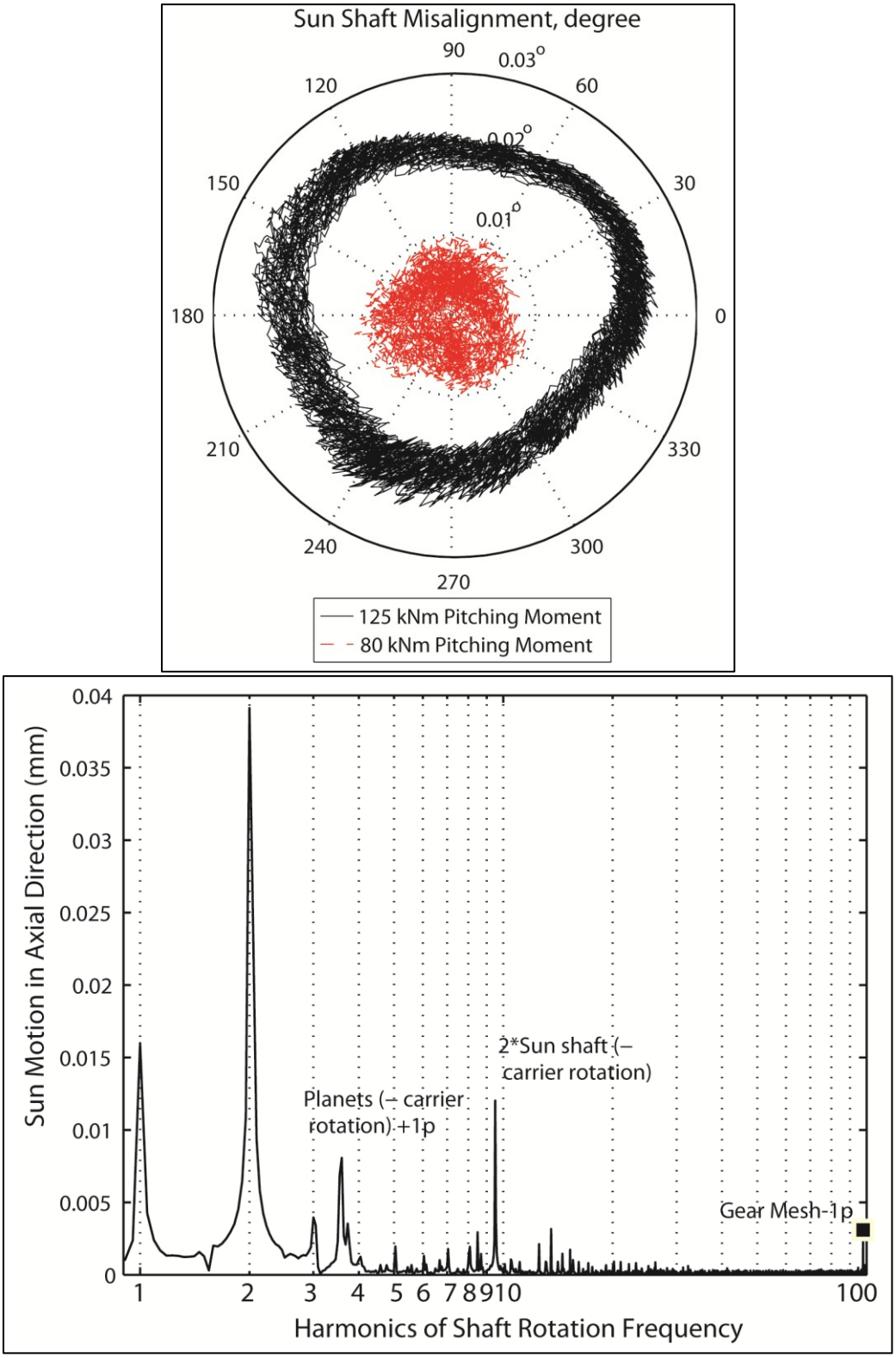

Figure 7. Measured sun gear orbit (top) and frequency spectrum (bottom)

3 Modeling Approaches

Three modeling approaches of varying fidelity are explored in this work: 1) an analytic model formulated in Section 3.1, 2) a hybrid, two-dimensional (2D) finite element (FE) and an analytic model described in Section 3.2, and 3) a fully three-dimensional (3D) FE model described in Section 3.3. The hybrid model (model 2) is RomaxWind 14.5.0 and the 3D FE model (model 3) is Calyx: Transmission3D version 2.2700|0.1195. These FE models of the drivetrain have previously been validated against relevant GRC experimental data for bearing and gear loading [2, 10-12].

3.1 Analytic Formulation

The analytic formulation described herein provides much of the same information as modern gearbox design software, plus estimation of spline safety factors. By its very nature, the formulation (model 1) provides greater insight into the effect of the spline coupling design parameters upon the spline performance and resulting safety factors than the other two approaches. Solutions can be calculated two orders of magnitude faster than higher fidelity models, making it very useful for early design stage parametric studies.

The analytic formulation was developed over many years by GEARTECH and was recently updated in a collaborative effort between GEARTECH and NREL. The formulation was also recently coded into MATLAB stand-alone software by NREL and then correlated by NREL and Romax Technology using the existing GRC models.

3.1.1 Assumptions

The major assumptions this analytic formulation makes are that:

- The hub and sleeve shafts are considered rigid. This assumption is valid most of the time because these shafts typically have large wall thicknesses to resist shaft twist. However, the analytical model could have conservative results than a model that accounts for compliance of the connecting shafts.
- Only angular misalignment is considered. This assumption is valid, at least for the GRC gearbox, because there was no strong evidence that the spline teeth were moving radially and contacting the roots during its inspection.
- Only torsional loading is considered. Radial gear loads are not included because, at least for the GRC gearbox and other common wind turbine gearboxes, they are reacted by bearings supporting the hollow shaft.
- The crowning of the spline teeth leads to constant base pitch spacing in all planes.
- The bending and contact stiffnesses are derived at a specified, steady torque, and tooth contact occurs only on the drive-side.
- The spline teeth are equally spaced circumferentially.

3.1.2 Stiffness of a Single Tooth Pair

Spline tooth bending stiffness is estimated using an analytical approach [13], considering combined tooth deformations caused by bending and compression. Line contact at the pitch

diameter is assumed. The actual bending stiffness may be somewhat different because the contact is conformal between two identical involute curves. The empirical values are based on measured deformation of gear teeth, rather than gear coupling teeth, under known test loads in which the tooth contact is localized near the pitch line. The spline tooth bending stiffness is:

$$C = FE\frac{Z_1 Z_2}{Z_1 + Z_2} \tag{1}$$

where the elasticity form factors are [13]:

$$Z_1 = \frac{Y_1}{0.76 + 7.25Y_1} \quad Z_2 = \frac{Y_2}{0.76 + 7.25Y_2} \tag{2}$$

The FE models typically express stiffness in terms of the rotational stiffness of a single tooth pair rather than bending stiffness. For the purpose of comparing the analytical formulation to the FE models, this rotational stiffness of a single tooth pair can be approximated as:

$$k_R = CR^2 \cos^2(\phi) \tag{3}$$

3.1.3 Hertzian Stress

Given that the curvature in the tooth profile direction is the same on both the hub and the spline, the Hertzian contact is modeled as a cylinder with radius R_F and length h_1 contacting on a semi-infinite plane. The contact stress is [15]:

$$\sigma_c = 0.418\left(\frac{P_i' E}{R_F}\right)^{1/2} \tag{4}$$

where the load per unit length is:

$$P_i' = \frac{P_i}{h_1} \tag{5}$$

and where the active tooth flank height is:

$$h_1 = \frac{D_o - D_i}{2} - h \tag{6}$$

The total normal tooth load is:

$$P_t = \frac{T}{R\cos(\phi)} \tag{7}$$

where the pitch radius equals:

$$R = \frac{N}{2P} \tag{8}$$

3.1.4 Bending and Shear Stress

The difference in bending and shear stress between a line contact model with a conformal contact model is expected to be insignificant because the total load carried by the tooth is the same. Assuming line contact at the pitch diameter, the gear coupling bending stress is:

$$\sigma_b = \frac{W_t P}{K_v F J} \tag{9}$$

The velocity factor is assumed to be equal to 1 in this study. The tangential force is:

$$W_t = P_i \cos(\phi) \tag{10}$$

The geometry factor equals [14]:

$$J = \frac{Y_1 C_\psi}{K_f m_N} \tag{11}$$

Where the hub tooth AGMA stress correction factor is [14]:

$$K_f = H + \left(\frac{S_F}{\rho_F}\right)^L \left(\frac{S_F}{h_F}\right)^M \tag{12}$$

The empirical factors H, L, and M are:

$$H = 0.331 - 0.436\phi \quad L = 0.324 - 0.492\phi \quad M = 0.261 + 0.545\phi \tag{13}$$

Spline connections typically use spur teeth, therefore, m_N and C_ψ equal 1. The final form of the bending stress is:

$$\sigma_b = \frac{P_i \cos(\phi) P K_f}{F Y_1} \tag{14}$$

At the pitch line, the spline shear stress is:

$$\tau = \frac{P_i \cos(\phi)}{t_{c1} F} \tag{15}$$

3.1.5 Tooth Load Distribution

The normal tooth load carried by the teeth adjacent to the highest loaded tooth is assumed to be proportional to the difference $z_e - z$ [16]:

$$P_d = P_i \left(\frac{z_e - z}{z_e}\right) \tag{16}$$

The elastic tooth deformation of the highest loaded tooth equals:

$$z_e = \frac{P_i}{C} \tag{17}$$

The maximum tooth separation occurs at the teeth located 90° from the highest loaded tooth [16]:

$$z_o = \frac{R_c \tan^2(i)}{2\tan(\phi)} \tag{18}$$

Where the hub root crown radius is:

$$R_c = R_F \cos(i_d)\sin(\phi) \tag{19}$$

Therefore, the total load (or load capacity) of the spline is:

$$P_t = KqNP_i \tag{20}$$

For very accurate splines, the accuracy factor equals 1 as used in this study. For commercially accurate splines, the accuracy factor is less than 1.

3.1.6 Jam Angle

The jam angle, or maximum misalignment angle, defines the upper boundary of the spline shaft tilt. Couplings must be designed so that their jam angle is larger than the maximum misalignment expected during operation as stated in AGMA 6123-B06 [5]; however, no simple guidance is given in the standard to calculate the jam angle. The circumferential space between two adjacent sleeve teeth is limited by the amount of S_{c2}, that is,

$$2f_c \sin(i) + t_{c1}^* \cos(i) = S_{c2} \tag{21}$$

where:

$$f_c = R_F \sin(i) \tag{22}$$

$$t_{c1}^* = t_{c1} - 2R_F\left[1 - \cos(i)\right] \tag{23}$$

where the sleeve circular space width is given by:

$$S_{c2} = \frac{\pi}{P} - t_{c2} \tag{24}$$

Inserting equations (22) through (24) into equation (21) yields:

$$\left(t_{c1} - 2R_F\right)\cos(i) + 2R_F - S_{c2} = 0 \tag{25}$$

Therefore, the jam angle equals:

$$i_{\max} = \operatorname{acos}\left(\frac{2R_F - S_{c2}}{2R_F - t_{c1}}\right) \tag{26}$$

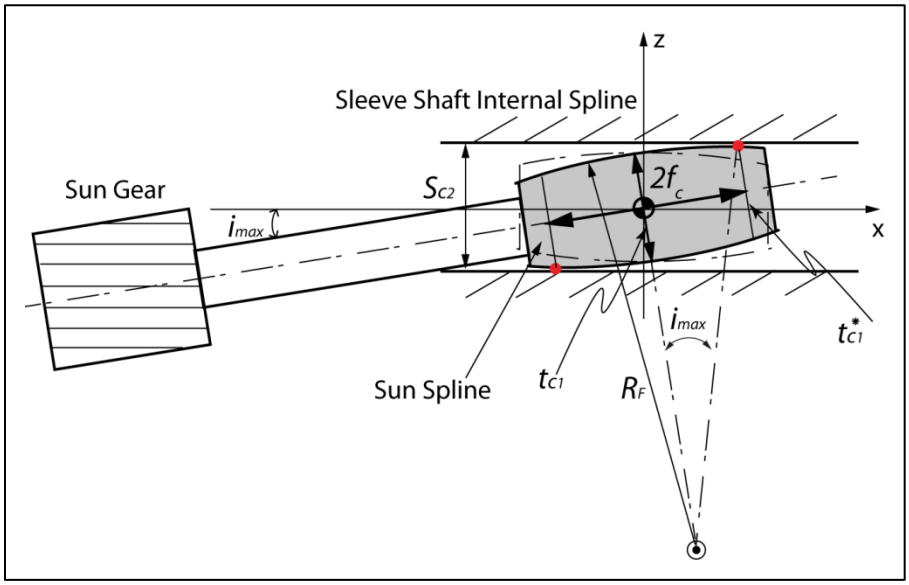

Figure 8. Misalignment spline contact on both sides of the tooth flank

However, equation (25) is only valid when $f_c \le F/2$. If the hub face crown radius is very large, it is possible that equation (22) will calculate that $f_c > F/2$. In this case, the contact point simply occurs at the edge of the spline and the jam angle is:

$$i_{\max} = \operatorname{asin}\left(\frac{F}{2R_F}\right) \tag{27}$$

Therefore, the final form of jam angle is the smaller of the quantities:

$$i_{\max} = \min\left\{\operatorname{acos}\left(\frac{2R_F - S_{c2}}{2R_F - t_{c1}}\right),\ \operatorname{asin}\left(\frac{F}{2R_F}\right)\right\} \tag{28}$$

Note that the jam angle is entirely determined by spline geometric parameters. It can be increased primarily by reducing the hub face crown radius or hub tooth thickness.

3.1.7 Strength Analysis

3.1.7.1 Fatigue Strength

For steel, the endurance limit of a beam specimen is:

$$S_e^{'} = 0.50 S_u \tag{29}$$

Applying factors for the spline geometry and operating conditions, the bending endurance limit is [17]:

$$S_e = K_a K_b K_c K_d K_e K_m S_e^{'} \tag{30}$$

Assuming the gear coupling is not subjected to torque reversals that are high enough to load the teeth in reverse bending, the fluctuating bending stress varies sinsusoidally from zero to the maximum bending stress:

$$\sigma_a = \sigma_m = \frac{\sigma_{b,\max}}{2} \tag{31}$$

from the modified Goodman's fatigue failure criterion:

$$\frac{\sigma_a}{S_e} + \frac{\sigma_m}{S_u} = \frac{1}{n} \tag{32}$$

If the safety factor is assumed to be 1 and the maximum bending stress is assumed to equal the bending endurance strength, the result is:

$$S_{bf} = \frac{2S_e}{1 + S_e / S_u} \tag{33}$$

For pure rolling, fatigue cracks initiate below the surface of Hertzian contact in the area of maximum shear stress. For rolling and sliding, the maximum shear stress moves to the surface. Juvinall [18] suggests the maximum shear stress exists at the surface when the coefficient of friction is greater than 1/9 and under the surface when it is less than 1/9. Spline connections typically have a coefficient of friction greater than 1/9 (AGMA 6123-B06 recommends 0.25); therefore, the surface-initiated fatigue case is considered here. It is assumed the coefficient of friction is 1/3 and Poisson's ratio is 1/4. The principal compressive stresses at the surface are then:

$$\sigma_1 = 1.39\sigma_c \quad \sigma_2 = 0.72\sigma_c \quad \sigma_3 = 0.53\sigma_c \tag{34}$$

The effective distortion energy stress is:

$$\sigma_e = \frac{\sqrt{2}}{2}\sqrt{(\sigma_1 - \sigma_2)^2 + (\sigma_2 - \sigma_3)^2 + (\sigma_3 - \sigma_1)^2} \tag{35}$$

Substituting equation (34) into equation (35), the final form of the effective distortion energy stress becomes:

$$\sigma_e = 0.782\sigma_c \tag{36}$$

The fluctuating contact stress varies sinsusoidally from zero to the maximum effective distortion energy stress, thus:

$$\sigma_a = \sigma_m = \frac{\sigma_e}{2} = \frac{0.782\sigma_c}{2} \tag{37}$$

Again using the Goodman fatigue failure criterion and assuming the safety factor is 1 and the maximum contact stress is equal to the contact endurance strength, the result is:

$$S_{cf} = \frac{2.56 S_e}{1 + S_e / S_u} \tag{38}$$

According to the maximum shear stress theory, the shear endurance strength is:

$$S_{sf} = \frac{1}{2} S_{bf} \tag{39}$$

3.1.7.2 Yielding Strength

Assuming Hertzian yielding occurs when the distortion energy stress equals the yielding endurance strength:

$$\sigma_e = S_y \tag{40}$$

and letting the contact stress equal the contact yield strength, the bending, contact, and shear yield strengths equal:

$$S_{by} = S_y \quad S_{cy} = 1.28 S_y \quad S_{sy} = \frac{1}{2} S_y \tag{41}$$

Spline connections can be made using different heat treatment processes. Table 3 summarizes the endurance and yield strengths for splines made from steel and heat treated by carburizing and nitriding and through hardening and induction hardening.

Table 3. Fatigue and Yielding Strength of Splines with Different Heat Treatment Processes

Strength (ksi)	Through hardened, H_B = 300	Carburized	Nitrided	Induction hardened, flank and root	Induction hardened, flank only
S_{bf}	62	83	65	81	33
S_{cf}	79	106	106	103	103
S_{sf}	31	42	33	41	17
S_{by}	130	140	140	120	120
S_{cy}	166	300	179	290	290
S_{sy}	65	70	70	60	60

3.1.8 Safety Factors

The safety factors based on fatigue are:

$$n_{bf} = \frac{S_{bf}}{\sigma_b} \quad n_{cf} = \frac{S_{cf}}{\sigma_c} \quad n_{sf} = \frac{S_{sf}}{\tau} \tag{42}$$

The safety factors based on yielding are:

$$n_{by} = \frac{S_{by}}{\sigma_b} \quad n_{cy} = \frac{S_{cy}}{\sigma_c} \quad n_{sy} = \frac{S_{sy}}{\tau} \tag{43}$$

3.1.9 Solution Methodology

The model is solved using numerical iterations and assuming an initial guess for q. The new value of q is calculated using the relationship curves [16]:

$$q = \begin{cases} 0.36\left(\frac{z_e}{z_o}\right) + 0.14 & 0.4 \le \frac{z_e}{z_o} < 1.0 \\ \left[1.195 + 1.75\left(\frac{z_e}{z_o}\right) - \left(\frac{z_e}{z_o}\right)^2\right]^{\frac{1}{2}} - 1.033 & \frac{z_e}{z_o} < 0.4 \\ 1 - \frac{1}{2\left(\frac{z_e}{z_o}\right)} & \frac{z_e}{z_o} \ge 1.0 \end{cases} \tag{44}$$

where the quantity z_e/z_o is a function of q and is calculated from equation (17). The preceding process iterates until the assumed q equals the calculated q within the specified tolerance (10^{-3} used in this study). The calculation process is described in Figure 9.

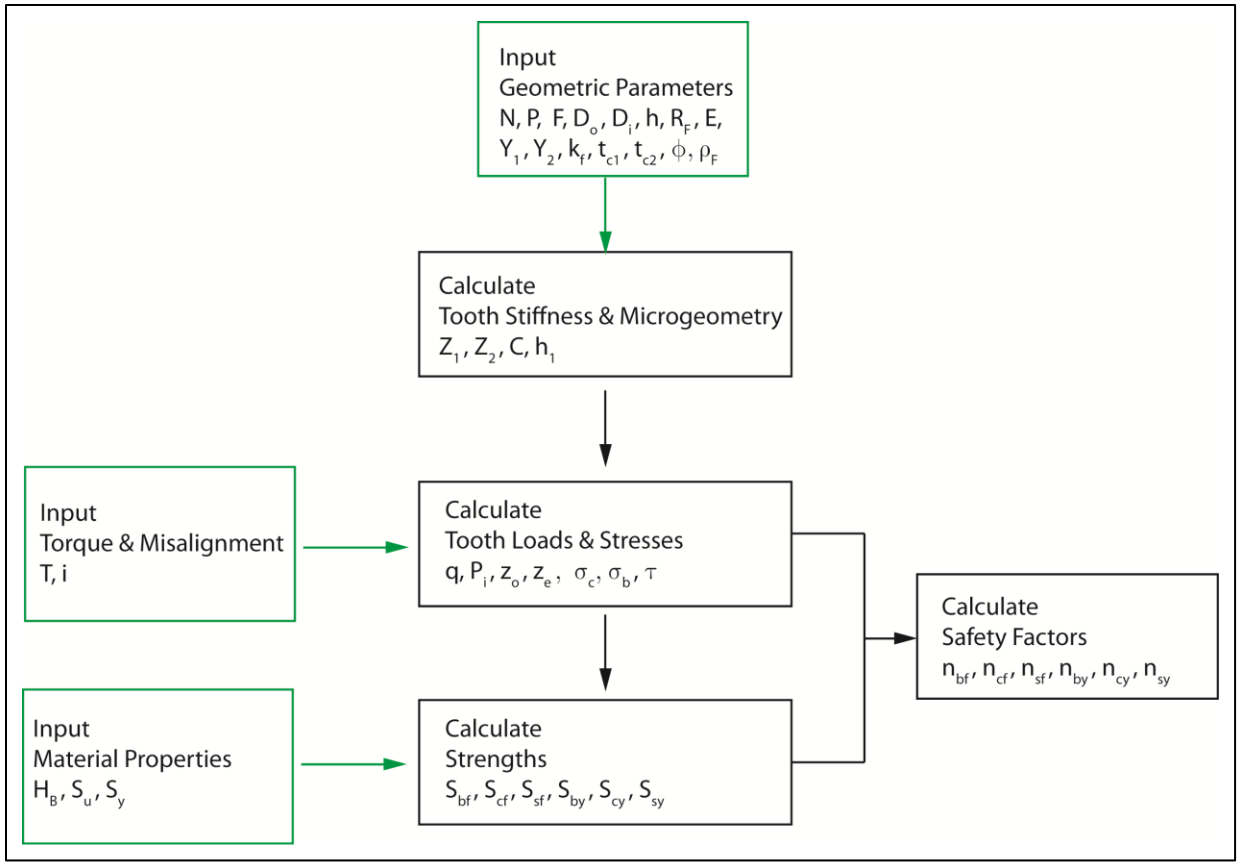

Figure 9. Flow chart of the spline stress, deformation, and safety factor calculations

3.2 Conformal Contact and Thin Strip Model: RomaxWind

The approach used in the commercial software package RomaxWind builds on an analytical foundation and then combines it with a numerical "thin-strip" model to capture the facewidth in contact. A key difference between the RomaxWind approach and the analytical and Transmission3D approaches described in this paper is that the contact is assumed to be conformal between the hub external teeth and sleeve internal teeth. The contact is assumed to occur at all points up the tooth height simultaneously. Local contact deformation is assumed to be negligible.

The first step in the approach is to determine the tooth stiffness per unit length assuming an unmodified, perfectly aligned spline. This stiffness is determined with a 2D finite element model of a single pair of teeth. The FE mesh is generated based on the parametrically defined tooth geometry. The rim thickness of the spline and hub meshes are used as specified for the true system. A unit load is applied to the inner rim of the hub, and the outer diameter of the sleeve is fixed. The contact is assumed to occur over the complete overlapping tooth profiles of the internal and external splines.

The spline is then broken into a finite number of lamina. Each lamina has a stiffness proportional to its width. The number of lamina in contact depends on the reduction in tooth thickness caused by crowning; the deflection caused by torque, radial forces, and tilting moment; and the misalignment. Pitch errors can also be included but are not provided in this analysis. The

deflections are iterated as part of a system nonlinear static analysis to find the position where the forces, moments, and deflections balance.

3.3 Line Contact and Three-Dimensional Finite Element Model: Transmission3D

The 3D finite element model in Transmission3D includes the flexibility of the spline teeth. For the purpose of comparing the 3D FE model to the analytical model, it can be configured to exclude the flexibility of the connection shafts. For the purpose of comparing it to the 2D FE model, it can be configured to include the flexibility of the connecting shafts. The model includes profile modification, lead modification, tooth spacing error, tooth flank flexibility, and rim flexibility. Assuming that the tooth contact is a line contact along the pitch line, the surface contact is solved by a surface integral approach that analyzes the near-field contact mechanics by integrating, in the style of a Green's function, the solution for a point load on a half space over the contact area [19]. FE analysis calculates far-field elastic deformations starting a small distance away from the contact area. Matching of the contact deflections and FE solutions at the matching surface yields a combined contact solution for near-field surface deformations [20, 21]. This FE model calculates tooth load share, load distribution, tooth deformation, contact stiffness, and contact stress.

4 Results and Discussion

The following sections evaluate the GRC sun shaft spline coupling using the developed analytical model, RomaxWind model, and the Transmission3D model considering both rigid and 3D FE shaft models. Because of the lack of experimental data, results of the analytic model formulation are simply compared to these outputs from the high-fidelity finite element models.

4.1 Spline Design Parameters

Two important spline design parameters are the rotational stiffness of a single tooth pair and the jam angle, which are compared for each model in Table 4. For the rotational stiffness, the analytical model predicts a significantly higher stiffness than the FE models that account for shaft flexibility and conformal contact. However, for the purpose of simply correlating the analytical model, the best comparison is with the Transmission3D rigid shaft model, because each model assumes line contact and a rigid shaft. In this case, there is only a 3% difference between the two models.

For the jam angle, the analytical model predicts an angle that is 50% higher than all of the FE models, which are in agreement with each other. The analytical formulation assumes a slightly different tooth profile shape than the FE models, which assume pure involutes. This different profile causes the difference in jam angles. The calculated jam angle for the GRC design of 0.20° is almost nine times the measured misalignment angle of 0.023° as shown in Figure 7. The GRC sun shaft 25.9-inch length tends to reduce the effect of the sun orbit; that is, for a given deflection of the sun, the longer the sun shaft, the lower the misalignment angle.

Table 4. Rotational Stiffness of a Pair of Spline Teeth

	Analytical	RomaxWind	Transmission3D: Rigid Shaft	Transmission3D: 3D FE Shaft
Rotational stiffness, Nm/rad	13.4×10^6	8.62×10^6	13.8×10^6	12.5×10^6
Jam angle, degree	0.30	0.20	0.20	0.20

4.2 Spline Loads

When the spline shaft is perfectly aligned with the sleeve shaft (hollow shaft), all of the teeth are in contact and the torque is transmitted evenly for ideally manufactured splines as shown in Figure 10(left). That is, the loads are centered on the facewidth and the maximum load on a single tooth equals the average load per tooth. However, when the sun shaft is misaligned, the number of teeth in contact is reduced, the loads migrate toward the edges, and the maximum tooth load increases significantly as shown in Figure 10(right). The variation of the loads is explored in the following sections.

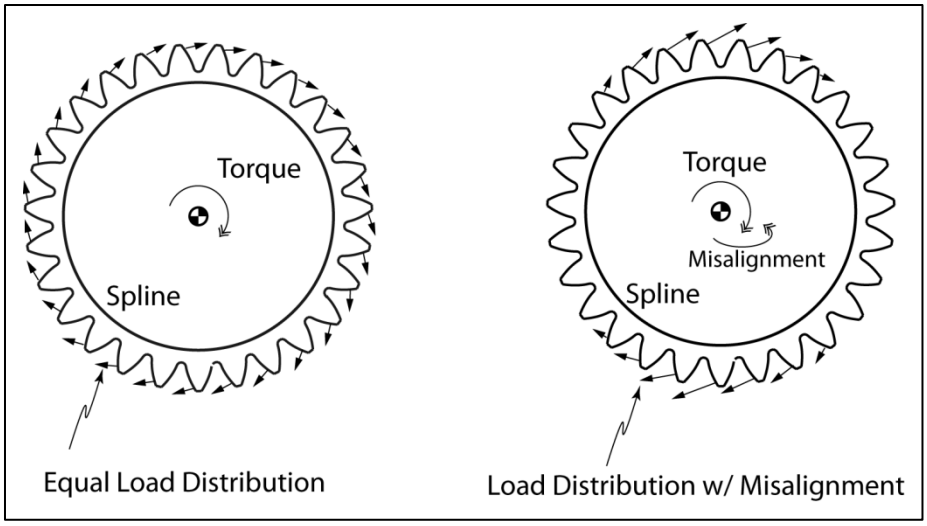

Figure 10. Tooth load distribution across spline teeth with (left) and without (right) misalignment

4.2.1 Effects of Shaft Misalignment

Figure 11 shows the effects of shaft misalignment angle on the number of teeth in contact and the maximum load on a single tooth at rated torque. In general, the analytical model agrees reasonably well with all of the FE models.

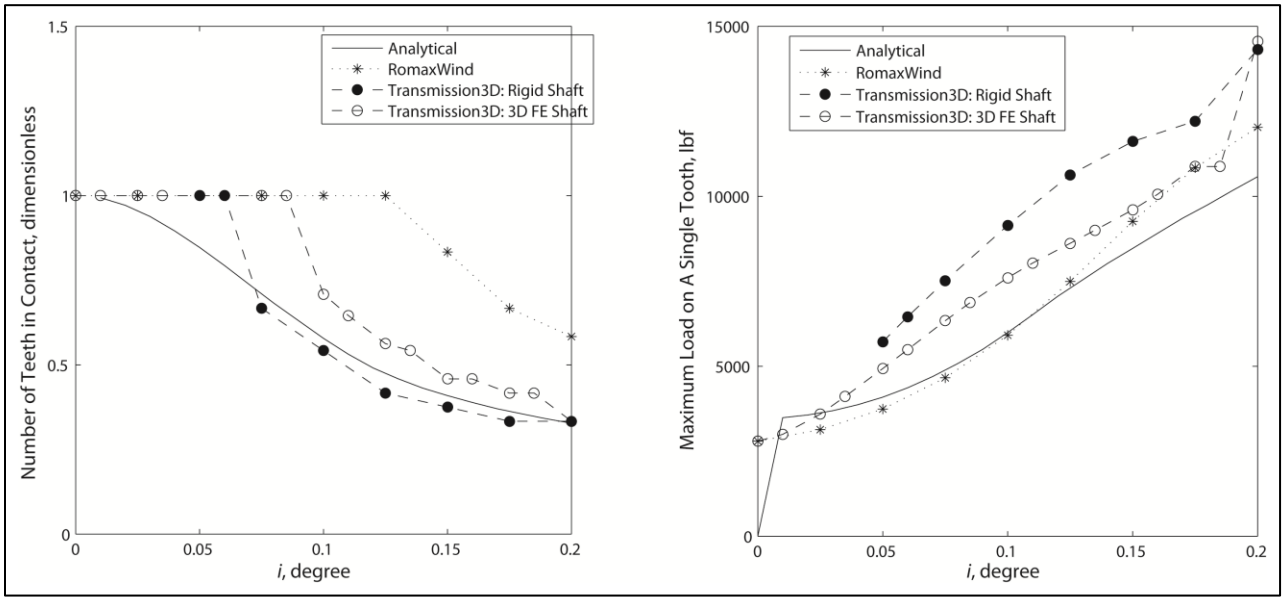

Figure 11. Effect of misalignment on the spline tooth loads

For the analytical model, an increase in the shaft misalignment from 0° to 0.2° (i.e., the jam angle) results in an immediate, but gradual decrease in the dimensionless number of teeth in contact from 1 to 0.36. At the jam angle, only 16 out of 48 teeth are in contact. The maximum load that a single tooth carries increases more than three times within the range of misalignment. The elevated tooth load increases the bending, contact, and shear stresses that could exceed their strength limits, leading to reduced service life.

The number of teeth in contact for the FE models does not immediately decrease with misalignment. This is a result of the inclusion of spline teeth and shaft elasticity and the subsequent additional compliance in the system. The misalignment angle at which the number of teeth in contact finally begins to decrease correlates with the amount of flexibility in the system. The fully flexible shaft models have the highest number of teeth in contact. However, at the jam angle the number of teeth in contact agrees reasonably well for all four models. Despite the fact that the number of teeth in contact is generally higher for the FE models than for the analytical model, the maximum tooth load for the FE models is also generally higher than the analytical model. This is especially evident at higher misalignment angles.

Figure 12 to Figure 14 show the tooth load distribution at rated torque at selected misalignment angles. Figure 12 is for the analytic formulation, Figure 13 is for the RomaxWind model, and Figure 14 is for the Transmission3D FE shaft model. The models are in good agreement, each capturing the influence of misalignment on the tooth load distribution.

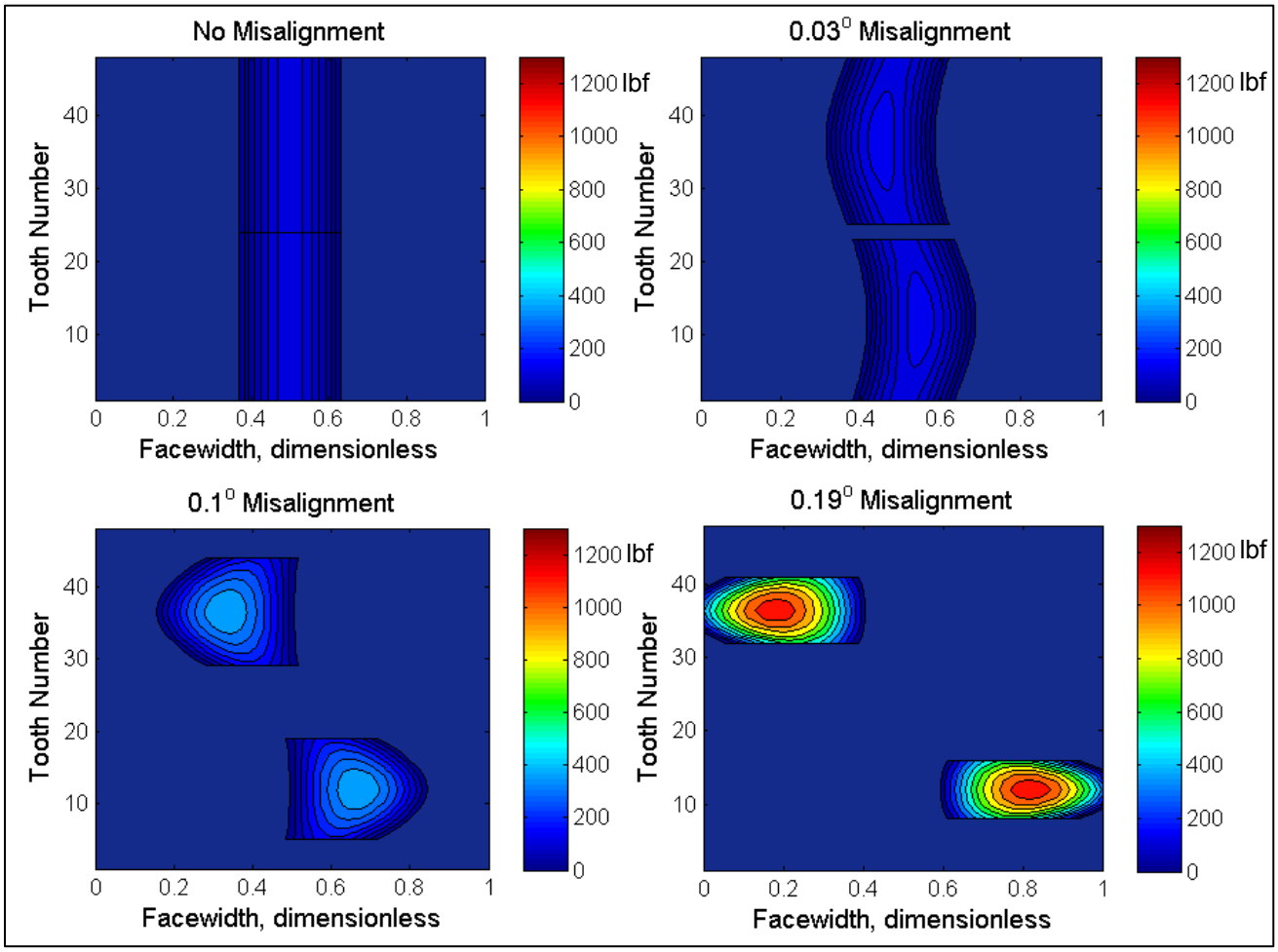

Figure 12. Spline tooth load distributions from the analytic model

When perfectly aligned, the teeth share loads equally, the tooth loads are centralized around the tooth facewidth center, and the load profile shape is parabolic. For small misalignment angles, the center of the contact area deviates from the tooth geometric center in a sinusoidal pattern

around the circumference of the spline. The further the center of the contact is from the tooth geometric center (center-to-center distance), the larger the tooth load is. As the misalignment angle grows, the center-to-center distance increases and so does the maximum tooth load. Near a misalignment angle of half the jam angle, some teeth are entirely unloaded. The remaining teeth in contact carry the load and their contact area migrates even closer to the tooth edge. At the jam angle itself, only about one-third of the teeth are carrying any load at all. In this situation, the maximum tooth load is approximately quadruple the nominal load and is located very close to the edge of the teeth. These edge-loaded teeth are at risk of pitting.

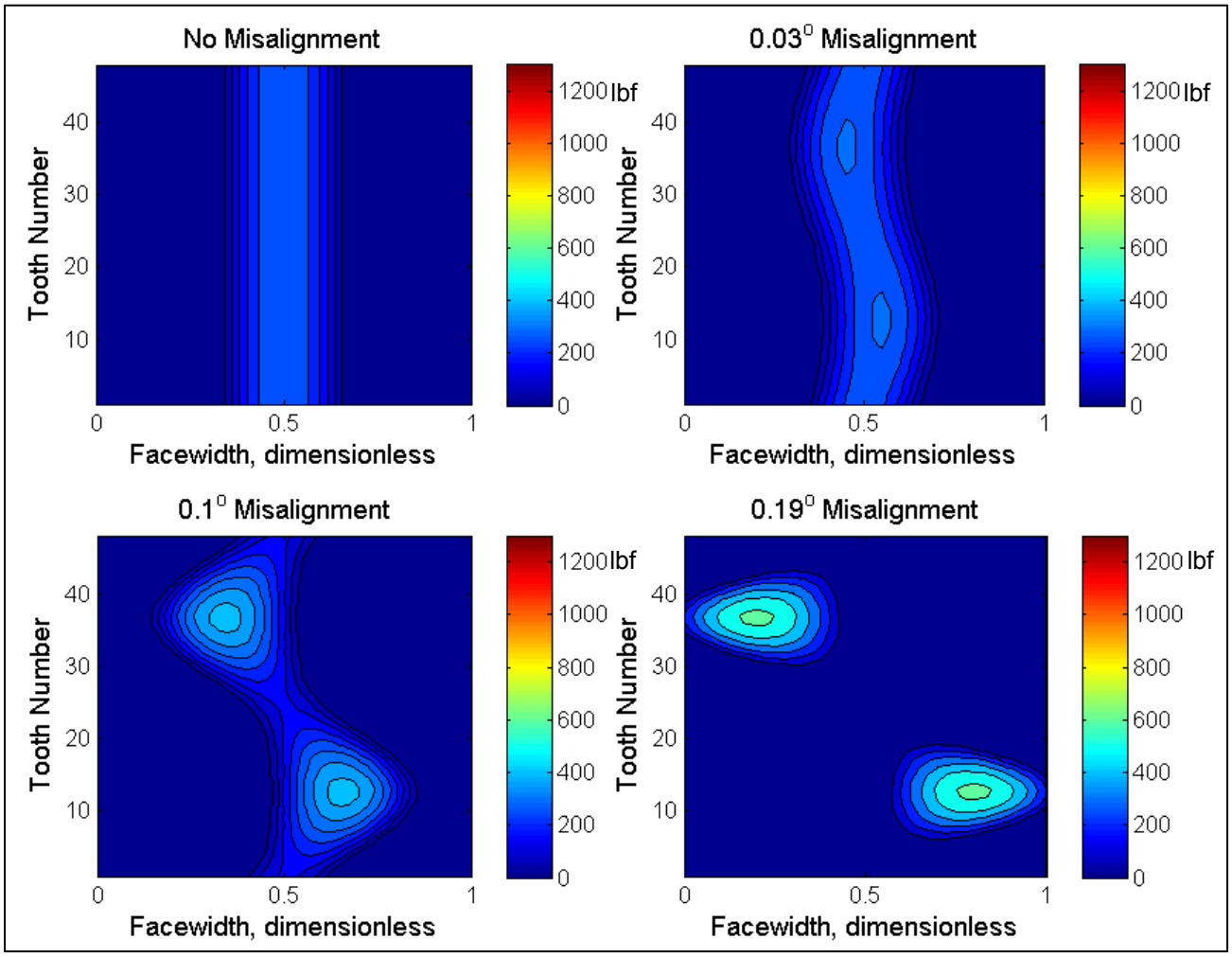

Figure 13. Spline tooth load distributions from RomaxWind

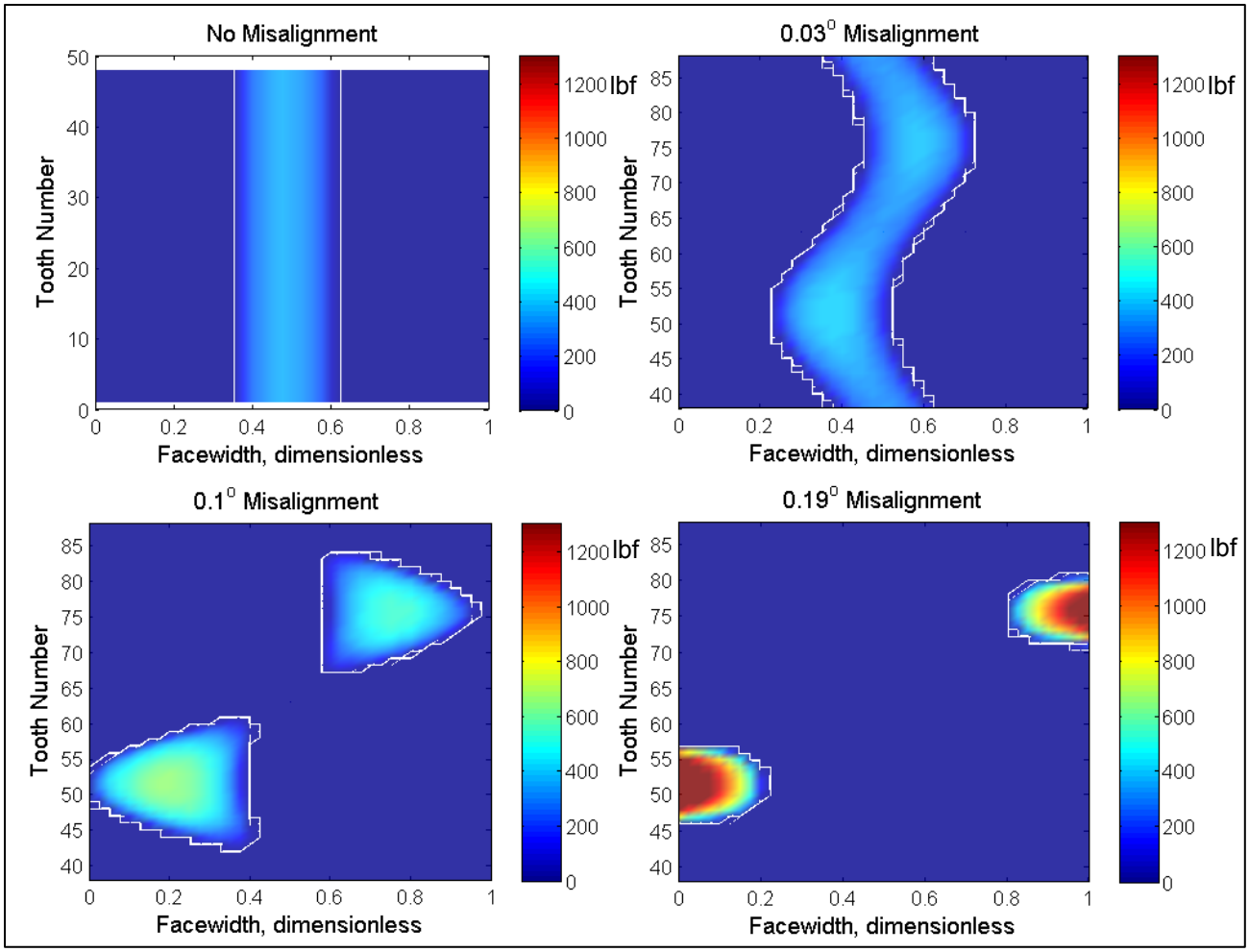

Figure 14. Spline tooth load distributions from Transmission3D

4.2.2 *Effects of Transmitted Torque*

The measured torque spectrum from field testing of the GRC gearbox in one turbine ranged from negative torque to two times the rated torque. The effects of torque on the number of teeth in contact and the maximum tooth load are shown in Figure 15. In these figures, the spline shaft is assumed to be misaligned by 0.1° (i.e., half the jam angle). The overall agreement among the models is acceptable.

The analytical model predicts lower maximum tooth loads than the high-fidelity models. This might be because of the simplification of the contact stiffness calculation of the proposed model. The proposed approach does not include the influence of torque on contact stiffness in equation (7) while the RomaxWind and Transmission3D models do include it. A safety factor of 1.5 is recommended for the analytical model for applications where the torque is less than 75% rated or greater than 125% rated. When torque increases from 50% to 150% of rated, the maximum tooth load for the analytical model approximately doubles as shown in Figure 15. The number of teeth in contact increases approximately 50% over this range. Therefore, spline loading and contact situations are clearly torque dependent. It is important to verify the spline design within the entire torque spectrum.

All of the FE results show similar trends with varying torque. The number of teeth in contact for the RomaxWind model is unaffected by torque over this range because of the high level of compliance in the system; however, the maximum tooth load correlates with the other models.With a rigid shaft, the Transmission3D model predicts the highest loads of all.

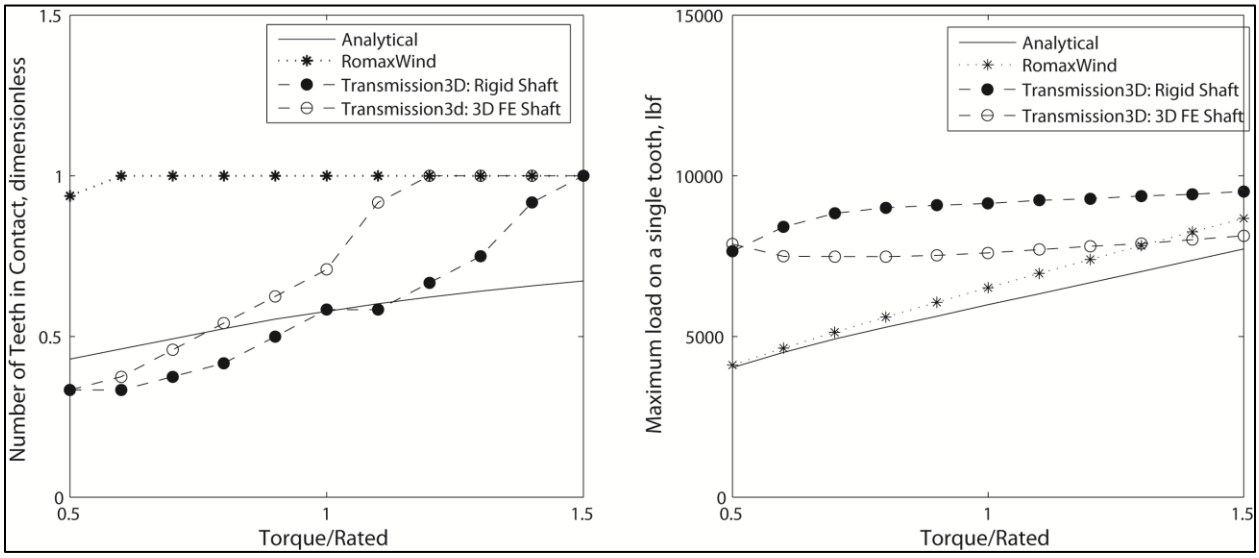

Figure 15. Effect of torque on the spline tooth loads

4.3 Spline Safety Factors

Safety factors compare the rated strengths of the spline against its bending, contact, and shear stresses in both fatigue and yielding. When the safety factor is less than 1, the spline stress exceeds its rated strength. When the safety factor is larger than 1, the spline design satisfies the strength requirement. The spline design is acceptable only when all of the safety factors are larger than 1.

The effects of shaft misalignment and transmitted torque on fatigue and yield safety factors are shown in Figure 16. The operating torque and misalignment values measured during the GRC dynamometer and field tests are highlighted in each figure. In general, the spline safety factors are well above 1. The bending safety factor based on yielding is low compared to the other yielding safety factors. However, even in the most extreme field conditions, this safety factor is still above 3. The bending safety factor based on fatigue can go below 1; however, this is only in high-torque and large misalignment conditions that would very rarely occur in the field.

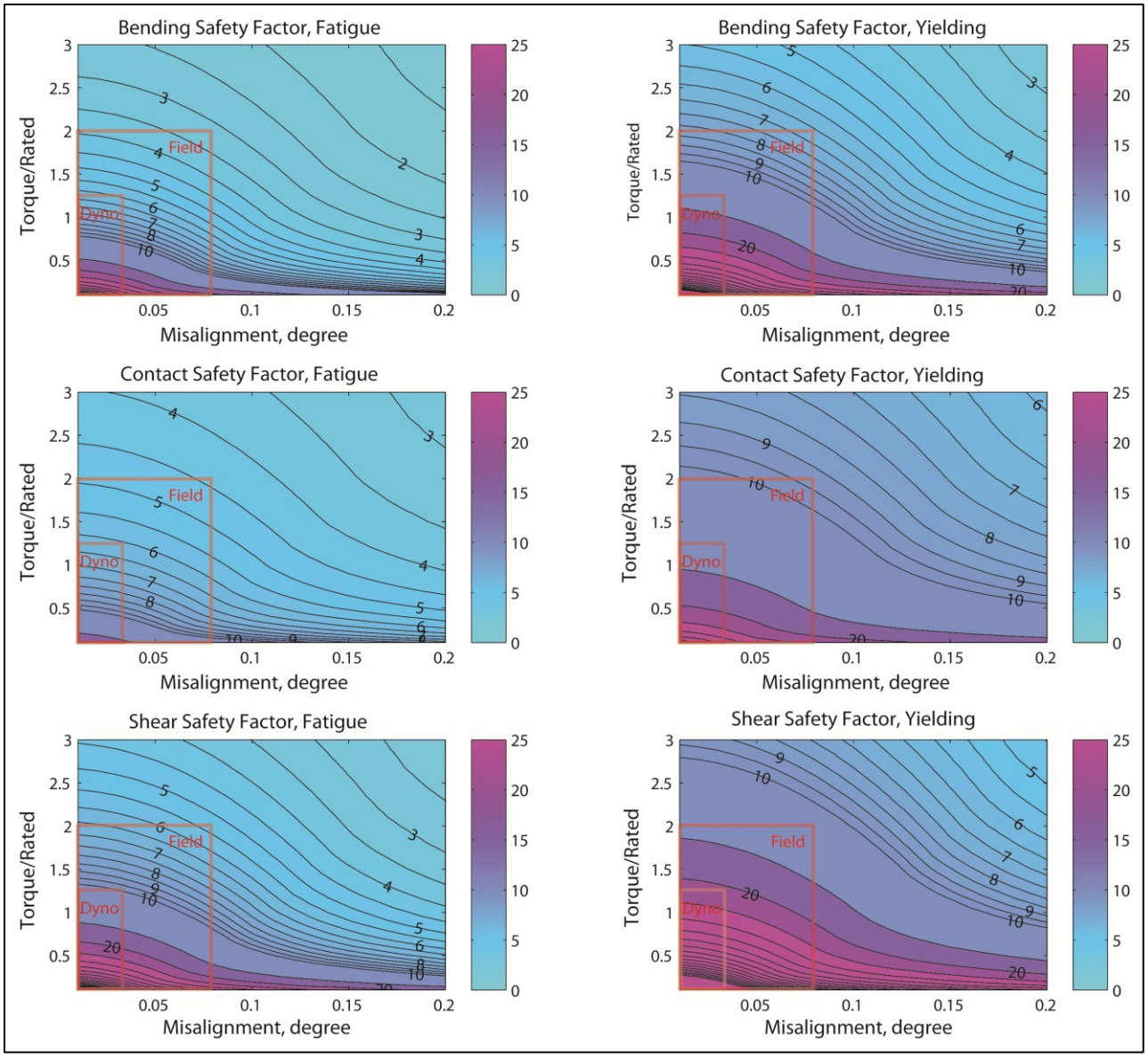

Figure 16. Effect of misalignment and torque on the spline safety factors

The GRC spline design meets all of the fatigue and yielding strength requirements; therefore, the spline damage shown in Figure 2 and Figure 3 is unlikely to have been caused by excessive loads or stresses. Although the spline meets all the strength requirements, the planetary section has poor load-sharing characteristics [2]. It could be possible to alter the design of the spline to both meet strength requirements and improve planetary section load sharing, essentially optimizing the spline design. This proposed model, together with the sun motion and torque measurements, can evaluate the spline's performance, possibly for use in real-time condition monitoring.

4.4 Gear Spline Coupling Program (Gear SCouP)

The analytic formulation described in this report was coded into MATLAB software and is available as a stand-alone program (i.e., a .exe) on an NREL-secure FTP website [**Error! Reference source not found.**]. The program itself is called the Gear Spline Coupling Program

(Gear SCouP) and the program graphical user interface (GUI) is shown in Figure 17. The input to the program includes spline dimensions, microgeometry, material properties, heat treatment, misalignment angle, and transmitted torque as described in Figure 9. These parameters are specified in an input data file called "input.txt" and can be read by SCouP by clicking the "Load Input File" button in the GUI interface. The "Review Input Parameter" button allows the user to review and edit these input parameters. Clicking the "Start Analysis" button initiates the analytic evaluation, normally requiring just a few seconds to complete the calculations. The program output consists of the spline stiffness, jam angle, spline load, plus contact, bending, and yielding stresses and their corresponding safety factors. The results can be plotted in the GUI screen by clicking the "Result Review" button or saved as an image file by clicking the "Capture Image" button. All of the input and output data can also be saved in a spreadsheet by clicking the "Save Result" button.

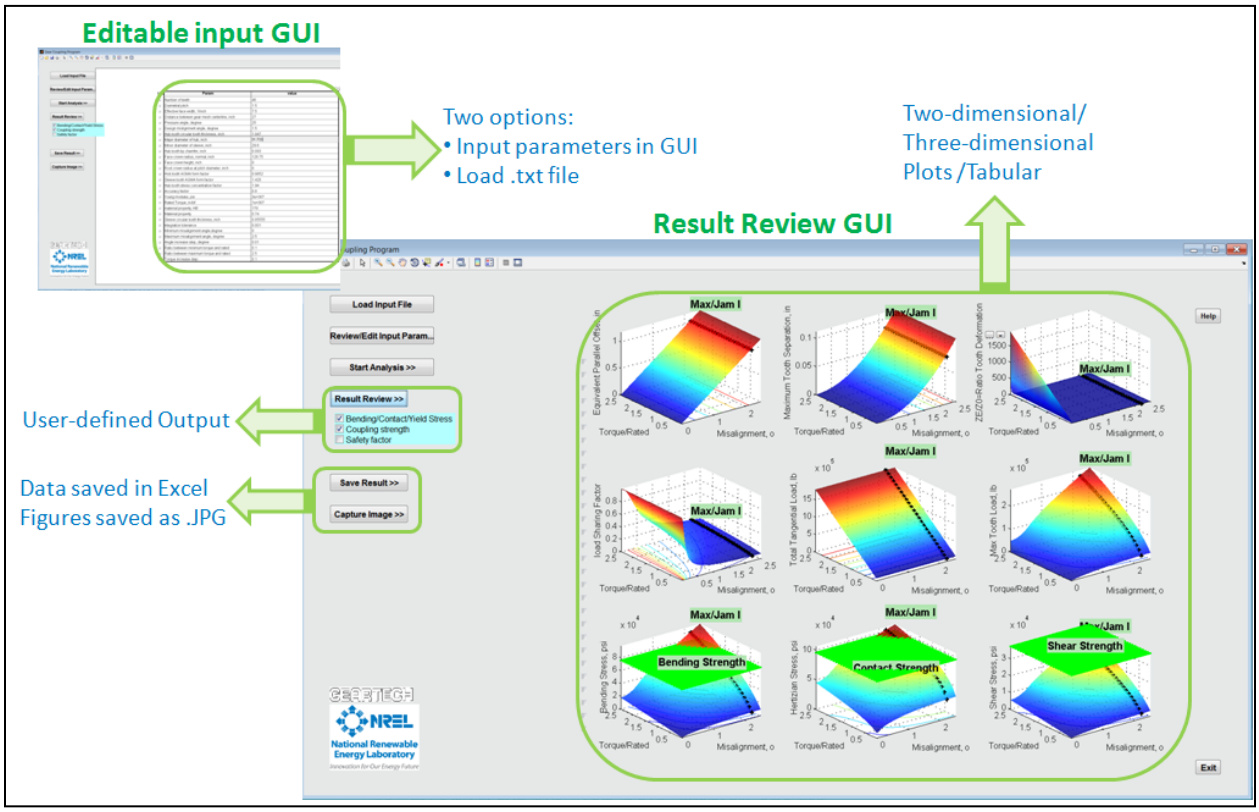

Figure 17. Gear SCouP graphical user interface

5 Conclusions

Splines are a critical but often overlooked part of the gearbox. In addition to the outright failure of the sun spline itself, poorly functioning splines could also be a contributor to failures in the rest of the planetary stage because of their influence on load-sharing characteristics. In this report, a new analytical model is described to evaluate spline designs commonly used in geared systems. Through this model, a greater understanding of the behavior of spline connections has been achieved and recommendations to improve design standards are summarized below.

5.1 Spline Modeling and Behavior

Evaluation of the spline design through direct measurements is extremely difficult; however, measurement of the sun orbit and resulting shaft misalignment is feasible. When combined with the developed model or high-fidelity FE models, the sun orbit measurement facilitates the best available evaluation of the spline design. The analytical model results compare favorably with high-fidelity FE analyses and quickly yield insights into relationships between the spline design parameters and resulting loads and stresses. Simulation time with the proposed analytical model is two orders of magnitude lower than high-fidelity FE analyses.

Given the spline properties, torque and shaft misalignment, the new analytic model calculates essential spline design information, including the jam angle, load share, maximum tooth loads, stresses, and safety factors. The sensitivity of spline loads, stresses, and safety factors to misalignment, transmitted torque, tooth crowning, and heat treatment was examined. Major findings from this study include the following:

- The spline jam angle is solely determined by geometric parameters and is independent of the modeling approach. Reducing the hub face crown radius increases the jam angle.
- When the spline is in perfect alignment, the load is shared equally across all spline teeth and the tooth load distribution has a parabolic shape. When the spline is misaligned, the number of teeth in contact decreases and the maximum tooth load increases sharply. The contact area deviates from the tooth center and moves toward the tooth ends. In the extreme, the spline teeth are edge loaded and at risk of failure.
- Torque affects the spline load share, maximum tooth load, and safety factors. It is important to evaluate the spline design within the entire torque spectrum.

5.2 Future Work

Future development of the analytic formulation and Gear SCouP will account for: 1) influences of the geometric spacing error of the hub and sleeve teeth on spline loads and stresses, 2) axial friction force that can cause unexpected forces and excitations, and 3) spline teeth life calculation, which is missing in current standards and literature.

5.3 Recommendations for Current Standards

Existing wind turbine gearbox design standards do not address spline design in great depth. In AGMA 6123, spline design is treated in terms of an allowable torque value based on semi-empirical models of shaft failure in shear and bursting (a failure mode in which the shell of the gear teeth ruptures), and spline tooth failure in shear at the pitch-line and wear [5]. These methods originate from the studies by Dudley [23] and Drago [24]. Assumptions are made

regarding the number of teeth in contact, the engaged spline length, and the load distribution factor. All of these parameters are essential for evaluating spline loads and stresses. The Gear-SCouP program calculates the values of these crucial parameters and their effect on safety factors, which can significantly increase the confidence in the spline design.

As described in Section 10.4.3 of AGMA 6123, the load distribution factor is 2 for misaligned splines with tooth crowning. That is, the allowable torque for a misaligned, crowned spline is reduced by half. However, this is an oversimplification. Misalignment and crowning have a nonlinear effect on the tooth load distribution and maximum tooth load. The Gear-SCouP program calculates the effect of misalignment and crowning on the resulting load distribution and maximum tooth load.

Additionally, other effects are mentioned in AGMA 6123 but are not explored. For example, crowning is mentioned in Section 10.4.4.3, which states that "external teeth should be crowned to avoid high end loading and to improve load distribution at the ends of teeth." However, the section also states "Crowning may reduce the load capacity of the coupling at zero degree misalignment, but improve the coupling life." It is clear that optimal tooth crowning is important for spline reliability, but no method is given to evaluate the effects of crowning. The GearSCouP program is suitable for performing a fast crowning optimization study during the gearbox design stage.

As stated in Section 10.4.8.2: "Couplings which will be misaligned must be designed with adequate radial and tangential clearance so that they will not jam at the maximum misalignment permitted by the design." However, a method to calculate the jam angle is not given. This study derives the jam angle and provides insight upon the relationship between the tooth geometry and jam angle. This formulation can reduce the number of iterations required to determine the spline geometry.

6 References

1. Sheng, S. *Report on Wind Turbine Subsystem Reliability - A Survey of Various Databases*. NREL/PR-5000-59111. Golden, CO: National Renewable Energy Laboratory, 2013.

2. Link, H.; LaCava, W.; van Dam, J.; McNiff, B.; Sheng, S.; Wallen, R.; McDade, M.; Lambert, S.; Butterfield, S.; Oyague, F. *Gearbox Reliability Collaborative Project Report: Findings from Phase 1 and Phase 2 Testing.* NREL/TP-5000-51885. Golden, CO: National Renewable Energy Laboratory, 2011.

3. Guo, Y.; Parker, R. G. *Dynamic Modeling and Analysis of a Spur Planetary Gear Involving Tooth Wedging and Bearing Clearance Nonlinearity*. European Journal of Mechanics A/Solids, vol. 29, pp. 1022-1033, 2010.

4. ANSI/AGMA/AWEA 6006-A03: Standard for Design and Specification of Gearboxes for Wind Turbines, ANSI/AGMA/AWEA, 2003.

5. ANSI/AGMA 6123-B06: Design Manual for Enclosed Epicyclic Gear Drives, ANSI/AGMA, 2011.

6. IEC/ISO, IEC International Standard 61400 Part 4: Design Requirements for Wind Turbine Gearboxes, 88/228/FDIS, 2012.

7. Errichello, R.; Muller, J. *Gearbox Reliability Collaborative Gearbox 1 Failure Analysis Report*. NREL/SR-5000-53062. Golden, CO: National Renewable Energy Laboratory, 2012.

8. Smolders, K.; Long, H.; Feng, Y.; Tavner, P. *Reliability Analysis and Prediction of Wind Turbine Gearboxes*. European Wind Energy Conference, Warsaw, Poland, 2010.

9. Link, H.; Keller, J.; Guo, Y.; McNiff, B. *Gearbox Reliability Collaborative Phase 3 Gearbox 2 Test Plan*, NREL/TP-5000-58190. Golden, CO: National Renewable Energy Laboratory, 2013.

10. Guo, Y.; Keller, J.; LaCava, W. *Combined Effects of Input Torque, Non-Torque Load, Gravity, and Bearing Clearance on Planetary Gear Load Share in Wind Turbine Drivetrains*. NREL/TP-5000-55968. Golden, CO: National Renewable Energy Laboratory, 2012.

11. Austin, J. *A Multi-Component Analysis of a Wind Turbine Gearbox using A High Fidelity Finite Element Model*. Ohio State University, Columbus, OH, 2013.

12. Crowther, A.; Ramakrishnan, A.; Zaidi, N. A.; Halse, C. *Sources of Time-varying Contact Stress and Misalignments in Wind Turbine Planetary Sets*. Wind Energy, vol. 14, no. 5, pp. 637-651, 2011.

13. Buckingham, E. Analytical Mechanics of Gears. Dover Publications, Inc, 1949.

14. AGMA 908-B89 Information Sheet: Geometry Factors for Determining the Pitting Resistance and Bending Strength of Spur, Helical and Herriongbone Gear Teeth, AGMA, 1989.

15. Timoshenko, S.; Goodier, J. N. Theory of Elasticity. McGraw-Hill, 1951.

16. Renzo, P. C.; Kaufman, S.; De Rocker, D. E. *Gear Couplings*. Journal of Engineering for Industry, pp. 467-474, 1968.

17. Shigley, J. E. Mechanical Engineering Design. Mc-Graw-Hill, 1977.

18. Juvinall, R. C. Stress, Strain, and Strength. Mc-Graw-Hill, 1967.

19. Vijayakar, S.M.; Busby, H.; Wilcox, L. *Finite Element Analysis of Three-Dimensional Conformal Contact with Friction*. Computers and Structures, vol. 33, no. 1, pp. 49-61, 1989.

20. Vijayakar, S. M. *A Combined Surface Integral and Finite-element Solution for a 3-dimensional Contact Problem*. International Journal for Numerical Methods in Engineering, vol. 31, no. 3, pp. 525-545, 1991.

21. Guo, Y.; Parker, R. G. *Stiffness Matrix Calculation of Rolling Element Bearings Using a Finite Element/Contact Mechanics Model*, Mechanism and Machine Theory, vol. 51, p. 32–45, 2012.

22. GRC FTP site, https://pfs.nrel.gov

23. Dudley, D. W. *When Splines Need Stress Control*. Product Engineering, p. 56-61, 1957.

24. Drago, R. J. *Rating the Load Capacity of Involute Spline*. Machine Design, p. 104-109, 1976.